Chapter 4

Methods

4.1 P receiver function method

Seismic phases converted from *P* to *S* underneath the receiver are particularly useful in studies of the crust and mantle (Figure 4.1). Due to the lower velocity of *S* waves in comparison to *P* waves, the converted *S* waves arrive after the onset of the direct *P* wave within the *P* wave coda. By extracting the small *P*-to-*S* (*Ps*) converted energy from the large *P* wave and measuring the time delay between the two phases it is possible to "map" seismic discontinuities beneath stations.

The frequency band of teleseismic body waves covers the range of one to several seconds and thus lies between controlled source methods (several Hertz) and surface-wave methods (many seconds).

The theoretical background of the technique was described e.g. by *Vinnik* (1977), *Burdick and Langston* (1977), *Langston* (1979), *Owens et al.* (1984), *Kind and Vinnik* (1988), *Kosarev et al.* (1993), and *Zandt et al.* (1995).

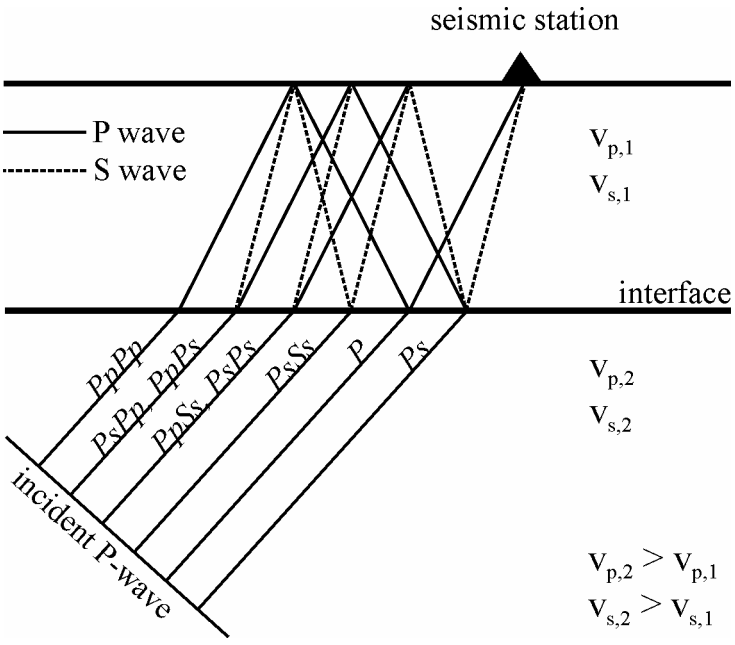

Figure 4.1: Sketch of a model with a horizontal layer over a half space. A plane *P* wave is incident upon the interface from below and generates *P*-to-*S* converted waves and many reverberations between the free surface and the interface.

The essential points in processing the observed data are:

1. If data from different types of seismic sensors and/or short-period seismic stations with different frequency responses are used, as is the case in the present investigation, it is necessary to restitute the broad-band ground displacement in order to make the signals better comparable. However, restoring longer periods from short period instruments is only possible for large magnitudes and depends on the transfer function of the sensor and the sampling rate. Furthermore, long period noise is also increased by restitution. The main frequencies of teleseismic body waves lie between 1 Hz and 0.1 Hz. High-pass filtering may be necessary after restitution to suppress long period noise.
2. Rotation of the original Z, NS and EW components of the *P*-wave group into the ray coordinate system *L*, *Q* and *T*. *L* contains mainly *P*-energy, *Q* mainly *SV*-energy, and *T* mainly *SH*-energy. The theoretical back azimuth is used to determine the radial component, and the angle of incidence is determined from the radial-vertical covariance matrix of the *P*-signal of the original data. The *Q*-component contains the information of main interest for this investigation: the *P*-to-*SV* converted energy. This energy depends mainly on the *S*-velocity distribution underneath the station (*Kind et al.*, 1995).
3. Deconvolution of the *Q*- and *T*-components with the *P*-signal on the *L*-component in the time domain. Deconvolution is used as a source-equalization procedure because it excludes effects of the rupture process and of the ray-path below the converting interfaces. Differences in the source durations and magnitudes are equalized, permitting the summation of many different events. Amplitude ratios are preserved by this procedure. The *P* waveform on the *L*-component is used to generate the time-domain wave shaping deconvolution filter. After deconvolution, all components are normalized to the maximum of *L* (*Kind et al.*, 1995).
4. Summation of many events from a large distance and azimuth range. Before summation, the data are corrected for distance move-out for direct *P*-to-*S* conversions using the *IASP91* reference model (*Kennett*, 1991; *Kennett and Engdahl*, 1991) and a standard slowness of 6.4 s per degree, corresponding to a reference epicentral distance of 67° (*Yuan et al.,* 1997). Thus, summation of records from different distances is possible in order to improve the signal-to-noise ratio and therefore the stability and reliability of the observations.

The processed receiver functions are usually filtered in order to enhance signals and to suppress noise. The choice of an inappropriate filter can heavily influence the information contained in the recorded data. Since the recorded signals have to be assumed to be mixed-phase, the processing of the data avoids pre-filtering of the data.

The receiver function technique has been successfully applied in numerous studies to investigate the crustal and upper mantle structure at regional scale, e.g. in central Europe (*Kind et al.*, 1995; *Grunewald et al.* 2001; *Wilde- Piórko et al.*, 2005), in Tibet (*Yuan et al.*, 1997; *Kosarev et al.*, 1999, *Kind et al.*, 2002), in North America (e.g. *Ramesh et al.*, 2002; *Rychert et al.*, 2005)), in the Middle East and North Africa (*Sandvol et al.*, 1998; *Hofstetter and Bock*, 2004), for the Hawaiian and other oceanic mantle plumes (*Li et al.*, 2000; *Li et al.*, 2003a) and in the Andes (*Yuan et al.*, 2000, 2002).

The classic receiver function technique used in the present study neglects indications of anisotropy of the earth medium. Signals in the *T* (transverse) component of the receiver function are usually explained by lateral heterogeneity of the isotropic medium, in particular, by dipping layers (*Langston*, 1979; *Savage*, 1998). By stacking receiver

functions from different distances and directions, effects of lateral structural variation are suppressed, and an average crustal model is obtained.

If a crustal velocity model is known for the investigated area, crustal thickness can be calculated from the measured delay times of the Moho *Ps* conversion. However, the crustal thickness estimated only from the delay time of the Moho *P*-to-*S* converted phase trades off strongly with the crustal v_p/v_s ratio. The ambiguity can be reduced significantly by incorporating the later multiple converted phases, namely, the *PpPs* and *PpSs+PsPs* (*Zandt et al.*, 1995, *Zhu and Kanamori,* 2000) (see Figure 4.1). In this thesis, the method of *Zhu and Kanamori* (2000) was used to calculate the depth of the Moho and the average crustal v_p/v_s ratio. In their grid search algorithm, the best estimations of crustal thickness and v_p/v_s ratio are found when the three phases are stacked coherently and thus reach the maximum-stacked amplitude. In this study, the grid search was carried out for Moho depths between 20 to 60 km and v_p/v_s ratios between 1.5 and 2.0. The direct *Ps* conversion from the Moho was weighted 0.5, the multiple conversions *PpPs* and *PpSs+PsPs* were each weighted 0.25 following the suggestions of *Zhu and Kanamori* (2000).

However, direct conversions and multiples sample different paths within the crust. The direct Moho conversions sample the Moho about 5-10 km away from the station, whereas the crustal multiples sample the Moho over a distance of 5-30 km from the station (*Zandt et al.*, 1995). By using average values over all back azimuths at single stations, a spatial low pass filter effect is obtained. Thus we get average crustal thicknesses beneath the stations.

4.2 S receiver function method

While the receiver function method analysing *P*-to-*S* conversions (*P* receiver function method) has been used successfully for quite a long time to investigate the crust and mantle structures, the study of *S*-to-*P* (*Sp*) conversions (Figure 4.2) is not a routine method yet. Although there are early works using *S*-to-*P* conversions (e.g. *Båth and Stefánnson*, 1966; *Burdick and Langston*, 1977; *Sacks and Snoke*, 1977; *Bock and Kind*, 1991), the use of these phases has only recently become more popular after receiver function analysis, meaning coordinate rotation and deconvolution, was also applied to the *S* waves in order to isolate the *S*-to-*P* converted phases from the incident *S* phases (*Farra and Vinnik*, 2000;

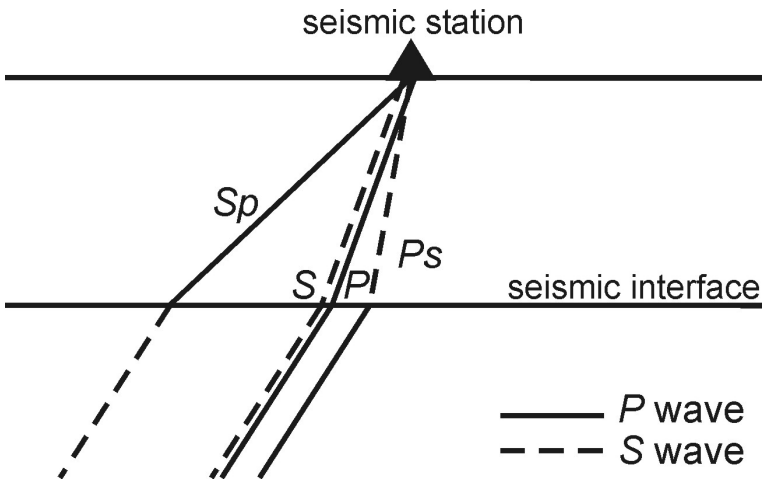

Figure 4.2: Ray paths of *Sp* and *Ps* converted phases.

Vinnik and Farra, 2002; *Vinnik et al.*, 2003; *Vinnik et al.*, 2004). Hence, this method is called *S* receiver function method. It was applied by *Li et al.* (2004), *Wittlinger et al.*, 2004; *Kumar et al.* (2005a, 2005b, 2006), and *Sodoudi et al.* (2006a, b) for mapping particularly the lithosphere-asthenosphere transition. A comprehensive overview about the *S* receiver function method applied to synthetic seismograms is given by *Yuan et al.* (2006).

As the converted *P* leg of the ray travels with a higher wave velocity than the direct *S* leg, *S*-to-*P* converted phases arrive at the receiver prior to the *S* wave onset, while the multiple reverberations appear after the *S* onset. Boundaries such as the lithosphere-asthenosphere transition, which are often obscured in the *P* receiver functions by crustal multiple reverberations arriving in the same time interval, can thus be better observed in the *S* receiver functions.

However, due to the ray geometry, the use of the *S* receiver functions has some limitations. Converted *Sp* phases from the lithosphere-asthenosphere boundary are best observed at epicentral distances between 60 - 85° (*Faber and Müller*, 1980; *Yuan et al.*, 2006). Beyond 85°, *SKS* waves arrive in front of *S*. *S* receiver functions are much noisier than *P* receiver functions, primarily because they arrive after the *P* wave. *S* waves have a lower frequency content, hence a lower spatial resolution than *P* waves.

The conversion coefficients of the Moho for *Sp* conversions are negative and of the lithosphere-asthenosphere transition positive, i.e. the sign of amplitudes is opposite to those of *Ps* conversions. The sign of amplitudes depends on the definition of Z components (downward positive), the sign of the velocity contrast at the discontinuities (downward positive at Moho, downward negative at lithosphere-asthenosphere transition) and the polarity of the triggering phase. The absolute conversion coefficients of *Sp* phases decrease with increasing epicentral distance (*Yuan et al.*, 2006). For epicentral distances of 60 - 85°, the conversion coefficient of the Moho varies between -0.165 and -0.12, and that of the lithosphere-asthenosphere transition between 0.043 and 0.024 (*Yuan et al.*, 2006).

In this study, *S* receiver functions were obtained from waveforms of *S* waves in order to investigate the lithosphere-asthenosphere transition. Initially, the broad-band ground displacement was restituted for the different seismic sensors.

The rotation into the ray coordinate system was performed in two steps. First, the seismograms in the *Z-N-E* System were rotated into the *Z-R-T* system using the theoretical back azimuth of the station-event combination. After this step a visual quality check was carried out: if the *R* component which contains most of the *SV* energy of the event showed *SV* energy at the time of the *S*-onset with a high signal-to-noise ratio, the event was chosen for further processing. If no *SV* energy was visible on the *R* component, the event was omitted (Figure 4.3). In the second step, the *Z* and *R* components of the mantle *S* phase are rotated into the ray coordinate system *L* and *Q* components, which contain the *P* and *SV* wave energy, respectively. The incidence angle for the rotation was determined by minimizing the amplitudes of *L* components at *S* arrivals.

Time domain wave shaping deconvolution of the *L* component with the signal on the *Q* component is then used for source equalisation and elimination of travel path effects. The resulting *L* component, which contains only *S*-to-*P* converted phases, is named *S* receiver function. Thus, 1043 traces of *S* receiver functions have been obtained in this study.

Since *Sp* conversions are generally weak, we need the summation of many individual records. Before stacking of the data, moveout correction is applied to the obtained *S* receiver functions to correct for the time dependence with epicentral distance. A reference slowness of 6.4 s/° and the IASP91 reference model (*Kennet and Engdahl*, 1991) are used. The time axis and sign of amplitudes are reversed so that the *S*-to-*P* conversions have positive arrival times and can be compared to the results of *P* receiver function analysis.

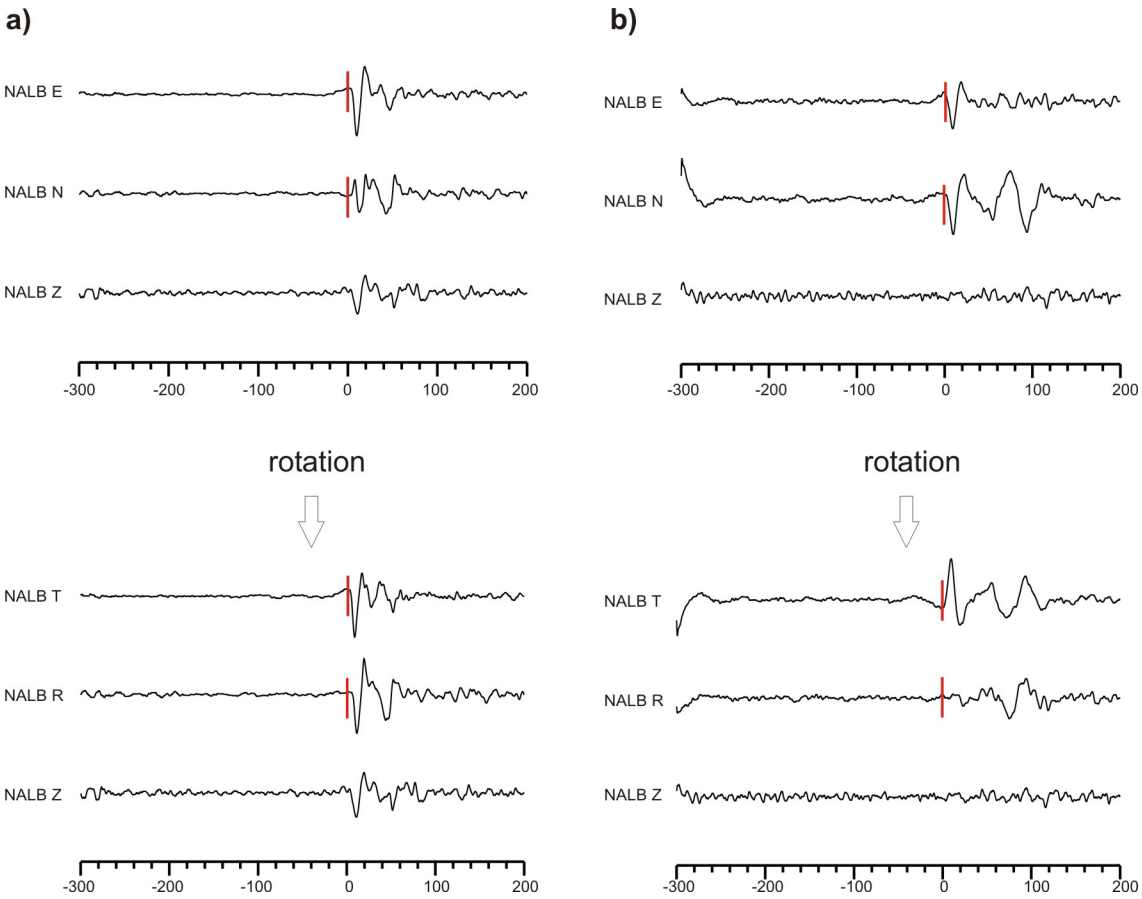

Figure 4.3: Rotation from the *Z-N-E* system into the *Z-R-T* system by theoretical back azimuth. After this step, a quality check of the data was carried out regarding the signal-to-noise ratio of *SV* energy on the *R* component. The time axis is set to zero at the time of the *S* onset. **a)** strong *SV* signal on *R* component at the time of the *S* onset, therefore the event is chosen for further processing. **b)** weak *SV* energy on the *R* component, event is omitted.